APPLIED SCIENCES AND ENGINEERING

Single-molecule polarization microscopy of DNA intercalators sheds light on the structure of S-DNA

Adam S. Backer[1]*, Andreas S. Biebricher[2], Graeme A. King[2], Gijs J. L. Wuite[2†], Iddo Heller[2†], Erwin J. G. Peterman[2*†]

DNA structural transitions facilitate genomic processes, mediate drug-DNA interactions, and inform the development of emerging DNA-based biotechnology such as programmable materials and DNA origami. While some features of DNA conformational changes are well characterized, fundamental information such as the orientations of the DNA base pairs is unknown. Here, we use concurrent fluorescence polarization imaging and DNA manipulation experiments to probe the structure of S-DNA, an elusive, elongated conformation that can be accessed by mechanical overstretching. To this end, we directly quantify the orientations and rotational dynamics of fluorescent DNA-intercalated dyes. At extensions beyond the DNA overstretching transition, intercalators adopt a tilted (θ ~ 54°) orientation relative to the DNA axis, distinct from the nearly perpendicular orientation (θ ~ 90°) normally assumed at lower extensions. These results provide the first experimental evidence that S-DNA has substantially inclined base pairs relative to those of the standard (Watson-Crick) B-DNA conformation.

INTRODUCTION

DNA conformation changes regulate structural maintenance, physical compaction, and access to stored information content within the genome (*1*). An understanding of the physical properties of DNA may advance rational drug design efforts (*2*) and lead to novel DNA-based materials (*3*). We seek to further uncover how base pair structure is altered as the DNA double helix (*4*) is mechanically stretched. It is well established that at 65 pN tension, bare DNA undergoes a cooperative conformation change, termed the overstretching transition (OST) (*5*, *6*). The OST is characterized by ~70% elongation of the DNA either due to base pair melting (*7*), by a conformation change from B-DNA to S-DNA (*8*–*12*), or by the coexistence of these two competing transitions. S-DNA is a base-paired (*8*, *9*), underwound conformation thought to have a helicity of ~37.5 base pairs per turn (*10*). Whether S-DNA is formed during overstretching depends on buffer ionic strength, base pair content, and temperature. However, further details regarding the structure of S-DNA have not previously been experimentally confirmed.

Intercalator fluorescence imaging has provided much insight into the phase transitions that accompany DNA overstretching (*7*, *9*, *13*–*16*). Intercalators are small molecules that bind between adjacent base pairs. Upon binding to DNA, intercalators locally unwind the double helix and lengthen base pair separation by 100%. π-Stacking interactions between intercalated chromophores and adjacent base pairs reduce intramolecular rotations and enhance fluorescence emission of intercalators by two to three orders of magnitude, enabling the optical detection of single intercalated dyes (*15*). In addition, intercalators preferentially interact with B-DNA over S-DNA (*9*, *16*) due to an energetic penalty incurred when intercalated DNA flanks S-DNA as opposed to B-DNA (*16*). These features have been leveraged to determine the factors affecting DNA melting versus S-DNA formation (*9*) and uncover a previously unconfirmed "hyperstretched" (HS-)DNA conformation (*16*).

Fluorescent molecules absorb and emit polarized light predominantly along the axis of their transition dipole moments (*17*). Hence, optical polarization, among other methods (*18*–*20*), may be used to directly determine the orientations of intercalated dyes (*21*–*24*). Since the DNA binding affinity and fluorescence enhancement of bound intercalators rely on π-stacking with neighboring bases, a measured dipole orientation of an intercalated dye will likely be a good indicator of the relative inclination of the flanking base pairs. Along these lines, van Mameren *et al.* (*24*) used a combined excitation/emission polarization technique to measure the response of intercalated dyes when DNA was stretched to different extensions using optical tweezers. That work revealed pronounced changes in fluorescence polarization as DNA was extended beyond the OST. However, the structural basis for this phenomenon remained unclear. By resolving this ambiguity, we provide important insight into the conformation of DNA under mechanical strain.

RESULTS

Experimental design

We devised a series of fluorescence polarization experiments that provide unprecedented access to both the orientation and rotational dynamics of intercalated dyes. Central to our approach is the use of dual-trap optical tweezers to align a DNA molecule (λ-phage; contour length $L_c \approx 16.5$ μm) within the image (x/y) plane of an epifluorescence microscope (*7*). Using an electro-optic modulator (EOM), we toggle between x and y polarizations of the fluorescence excitation laser. In such a manner, we alternately excite different populations of intercalated dyes with dipole moments aligned closer to the respective x/y axes of the imaging system (*23*, *25*–*27*). In addition, we deduce information about the orientations of the subset of preferentially excited dyes by resolving the x/y polarization components of the detected emission using a polarizing beamsplitter (see Materials and Methods) (*22*, *28*, *29*). The fluorescence polarization is computed as

$$ {}_xP = \frac{{}_xI_x - {}_xI_y}{{}_xI_x + {}_xI_y}; \quad {}_yP = \frac{{}_yI_x - {}_yI_y}{{}_yI_x + {}_yI_y} \tag{1} $$

[1]Sandia National Laboratories, New Mexico, P.O. Box 5800, Albuquerque, NM 87185-1413, USA. [2]Department of Physics and Astronomy, LaserLaB Amsterdam, Vrije Universiteit Amsterdam, De Boelelaan 1081, 1081 HV Amsterdam, Netherlands. *Corresponding author. Email: abacke@sandia.gov (A.S.Ba.); e.j.g.peterman@vu.nl (E.J.G.P.)
†These authors jointly supervised this work.

In Eq. 1, prefixes denote excitation polarization and suffixes denote emission polarization. ${}_{x,y}I_{x,y}$ refers to the fluorescence intensity recorded using x/y-polarized excitation in the x/y-polarized emission channel. ${}_{x,y}P$ refers to the fluorescence polarizations resulting from x/y-polarized excitation, respectively. Positive values of ${}_{x,y}P$ indicate molecular ordering along the x axis of the experimental reference frame, and negative values indicate alignment near the y axis.

Intercalator fluorescence depolarizes beyond the OST

Our initial experiments quantify the polarization response of the cyanine intercalator YOYO-1 (*30*) at different DNA extensions (*21*, *24*). Following previous work (*24*), in which changes in fluorescence polarization were first observed at extensions beyond the OST, DNA was extended in the presence of intercalators using a low-salt imaging buffer (see Materials and Methods). This buffer (where intercalator unbinding is much slower than the stretching speed) ensures a relatively high dye coverage that persists even during DNA overstretching (*16*). Note that despite the low-salt conditions, intercalation prevents melting and strand separation during the OST (see section S1).

We highlight three regimes within the force extension curves of DNA (Fig. 1B). We observe that both before and within the OST (regimes 1 and 2, respectively), fluorescence emission remains negatively polarized, and dyes are efficiently excited only using an excitation polarization perpendicular to the DNA axis (*21*, *24*). This indicates that intercalators align parallel to the DNA base pairs and perpendicular to the DNA axis (Fig. 1C). Notably, at extensions beyond the end of the OST (regime 3), the dye emission becomes depolarized, and either x- or y-polarized excitation yields fluorescence signal (Fig. 1D). On the other hand, at extremely high intercalator coverage—when the DNA undergoes a transition to the hyperstretched form (*16*)—intercalator fluorescence remains negatively polarized (indicating perpendicular alignment to the DNA axis), even at very high forces (beyond regime 3; see fig. S1 and section S2).

The observation of depolarized fluorescence beyond the OST (regime 3) as shown in Fig. 1D has been reported before by van Mameren *et al.* (*24*), who proposed two hypotheses to explain this unexpected change: (i) The orientation of an intercalator within its binding site may undergo rapid rotational diffusion in the time interval between

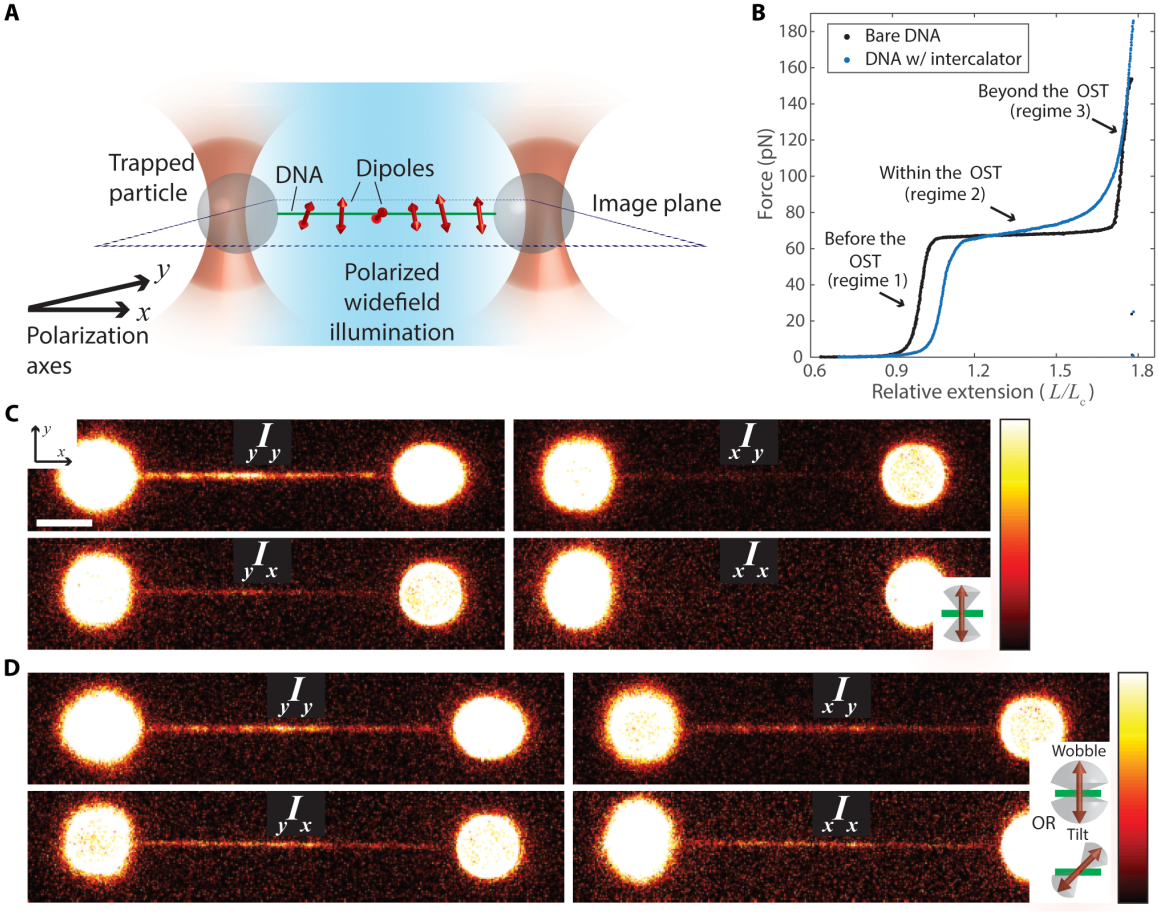

Fig. 1. Intercalated DNA fluorescence changes polarization after the OST. (**A**) Optical tweezers align and stretch a DNA molecule within the microscope image (x/y) plane. Polarized laser light excites intercalated dyes, and corresponding fluorescence is resolved into x- or y-polarized components using a polarizing beamsplitter. Dipoles of intercalated dyes are depicted as bidirectional arrows. (**B**) Typical force-extension curves for both bare DNA and DNA in the presence of ~10 nM YOYO-1. While the two curves differ slightly, in both cases, three distinct regimes can be distinguished: before the OST (regime 1), within the OST (regime 2), and beyond the OST (regime 3). (**C** and **D**) Fluorescence polarization images show DNA densely coated with YOYO-1, extended horizontally to regimes 2 and 3 [(C) and (D), respectively] (scale bar, 5 μm). Insets illustrate the possible intercalator dipole orientations (red) with respect to the DNA axis (green) that could induce the observed fluorescence polarization features. Gray cones depict wobble regions from which dipoles may depart from their mean orientations. Note that in the increased wobble hypothesis [upper inset of (D)], dipoles explore a greater range of orientations due to a wider wobble cone.

excitation and fluorescence emission. Such random reorientations or "wobble" may occur while the mean axial tilt with respect to the DNA axis (θ) remains close to 90°. (ii) Alternatively, the DNA base pairs may incline, compelling intercalated chromophores to tilt in concert—i.e., the mean axial tilt θ may change (see Fig. 2B for definitions of wobble and tilt). Previous measurements have not provided enough evidence to confirm or refute either hypothesis. In addition, some combination of tilting and increased probe wobble could be in effect. Moreover, two factors cause azimuthal variation of the dipole orientations with respect to the DNA axis: (i) the helicity of the DNA [3- to 20-nm pitch (*10*)] and (ii) Brownian twisting of the DNA [rotational correlation time of ~100 ns (*31*), without active manipulation of DNA twist (*32*)]. The temporal resolution (~s), the spatial (~250 nm) resolution, and the average intercalator spacing (≪250 nm) of these experiments result in cylindrical averaging over all possible intercalator dipole moment orientations, rendering prior experiments blind to azimuthal orientation with respect to the DNA axis.

Reorienting a stretched DNA molecule reveals that intercalators tilt

To determine the underlying cause of the depolarization observed in regime 3, we modify our experimental approach: Instead of stretching the DNA molecule horizontally, we extended the DNA along different angles ω within the image plane (Fig. 2A). Representative polarization images of DNA extended beyond the OST (regime 3) and oriented at ω = 45° are shown in Fig. 2C. The results contrast markedly with those of horizontally extended DNA shown in Fig. 1D: Under *x*-polarized excitation, the *x*-polarized emission channel records more signal than the *y* polarization channel, and *y*-polarized excitation induces *y*-polarized emission. Thus, by changing the orientation of the DNA from ω = 0° to ω = 45°, the dye emission in regime 3 switches from depolarized to polarized. If the tilted intercalator hypothesis is valid at extensions beyond the OST, then as the DNA is stretched horizontally (ω = 0°), tilted dipoles will align parallel neither to the *x* nor the *y* axis, leading to depolarized emission. However, at ω = 45°, a subset of the tilted dipoles is preferentially excited (insets, Fig. 2C), causing the emission to be polarized parallel to the excitation axis. If, alternatively, tilting is negligible, and dipoles are free to wobble loosely within their binding sites, then there would be no DNA orientation ω that would substantially increase the magnitude of the emission polarization beyond the values recorded at ω = 0° and ω = 45°. We therefore posit that substantial intercalator tilting occurs beyond the OST.

We next developed a theoretical model (see sections S3 to S5) to estimate the expected *x*/*y*-polarized emission intensity (and hence the emission polarization ratios ${}_{x,y}P$) for a given excitation polarization. This model calculates the orientation distribution of fluorescent probes and accounts for energy transfer between YOYO-1 chromophores (see section S6) (*24*, *33*, *34*). We assume (Fig. 2B) that each dipole is oriented at a mean angle θ with respect to the DNA axis, and the intercalated dipole orientations obey cylindrical symmetry about the DNA axis. In addition, to quantify rapid probe wobble (discussed above), we specify that a dipole may rotate about its mean orientation within a cone of half-aperture α. The parameter α may also account for other depolarization processes that occur on a time scale faster than the dye fluorescence lifetime, such as energy transfer. We have measured ${}_{x,y}P$ as a function of ω (Fig. 2, D and E) and fitted experimental data to our model to estimate the unknown parameters {θ, α} using nonlinear least squares estimation (see Materials and Methods). At extensions within the OST (regime 2) (Fig. 2D), we estimate θ = 85.4° ± 4.0°, α = 29.1° ± 4.5°—these estimates are

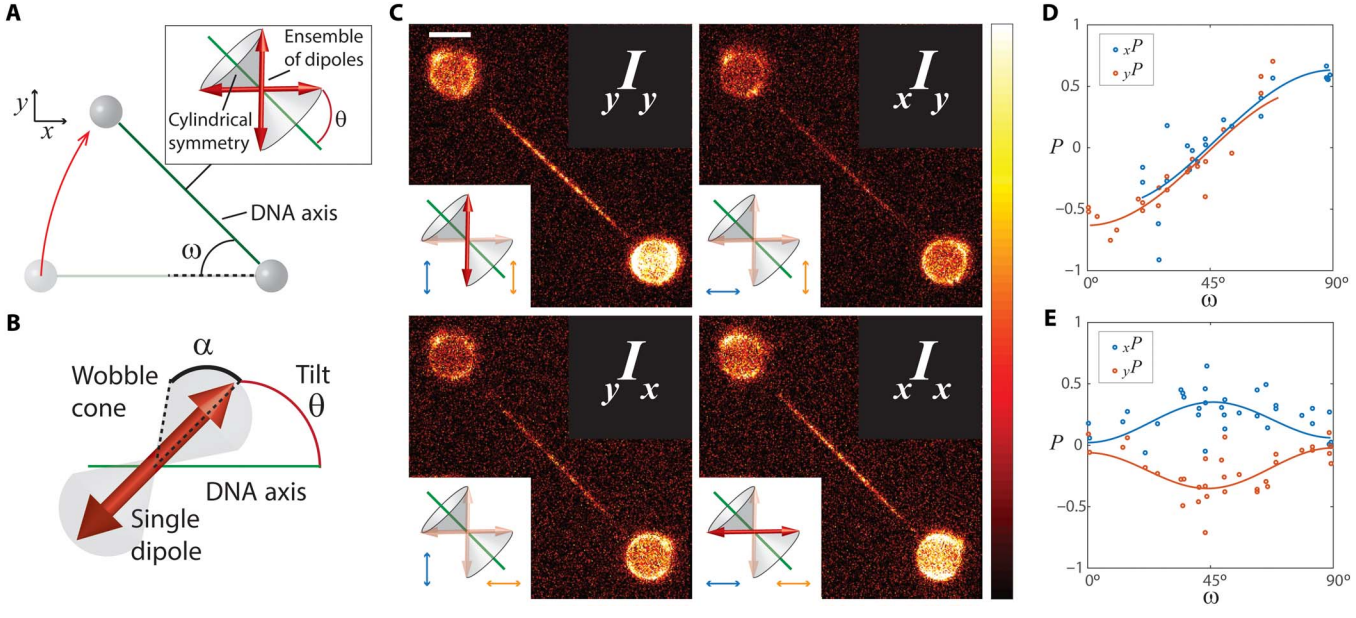

Fig. 2. Stretching beyond the OST induces DNA intercalator tilting. (**A**) By adjusting the DNA orientation (ω) within the image plane of the microscope, the axial tilt of intercalators can be distinguished from wobble. Cylindrical symmetry of dipoles about the DNA axis is assumed (inset). (**B**) Scheme on which the theoretical analysis is based, assuming two independent parameters (mean dipole tilt θ and wobble cone α). (**C**) Polarization images of DNA stretched to ~120 pN (regime 3), oriented at ω = 45° (scale bar, 5 μm). Insets illustrate how the laser polarization preferentially excites a subset of dipoles. Blue arrows denote excitation polarization axis, and orange denotes the emission polarization channel. When the excitation polarization is aligned with the emission channel polarization (upper left and bottom right images), greater signal is detected along the DNA. (**D** and **E**) Measured ${}_{x,y}P$ (dots) as a function of ω with corresponding fits (solid line) based on the theoretical model (see section S4) using parameters {θ = 85.4°, α = 29.1°} and {θ = 53.6°, α = 39.1°} for DNA extended within regimes 2 and 3 [(D) and (E)], respectively.

consistent with previous measurements (*22*–*24*) that predicted negligible dipole tilting (i.e., θ is nearly 90°). At extensions beyond the OST (regime 3) (Fig. 2E), we estimate θ = 53.6° ± 1.4°, α = 39.1° ± 1.9°, confirming intercalator tilting. We note that a fourfold degeneracy is present in our θ estimates [i.e., we do not distinguish between {53.6°, −53.6°, 126.4°, −126.4°}]. This ambiguity has two causes: Our theoretical model assumes cylindrically symmetric ordering of an ensemble of dyes about the DNA axis. Furthermore, both absorption and emission of fluorescence intensity of a given polarization are proportional to the cosine-square of the angle between the absorption/emission dipole moment and the angle of the excitation/analyzing polarization, respectively.

Our fitted data also show an increase in the cone angle parameter α of ~10°. However, it is unclear whether this result is indicative of enhanced dye rotational mobility or a combination of other rapid depolarization processes. Factors such as energy transfer between individual chromophores or adjacent YOYO-1 dyes may depolarize fluorescence emission, leading to a larger estimate of α (see sections S4 and S6 for an analysis of the capacity of our fitting procedure to distinguish changes in θ versus α and a discussion of effects related to energy transfer). In addition, a slight difference in orientation between the absorption and emission dipole moments of an individual chromophore may induce an increased estimate of α. For intercalators, absorption and emission dipole moments are generally thought to be nearly parallel (*30*). However, this potential source of depolarization cannot be completely ruled out. Last, it is possible that all dyes bound to the DNA construct do not assume an identical tilt θ with respect to the DNA axis. Nevertheless, the observed increase in the magnitude of ${}_{x,y}P$ at DNA orientations ω ~ 45° can only be attributed to preferential orientational ordering of dyes such that they are tilted away from the plane perpendicular to the DNA axis. The above-mentioned factors may influence our estimate of α; however, the reported mean axial tilt of θ ~ 54° is expected to be robust to these rapid depolarization processes.

Single-intercalator imaging demonstrates that intercalators twirl in addition to tilting

To verify that intercalator tilting occurs under a wide variety of experimental conditions, we reduced the density of intercalators and recorded single-intercalator fluorescence at a force of ~90 pN (regime 3; Fig. 1B). To ensure S-DNA formation under these low dye coverage conditions, a high-salt buffer was used (see Materials and Methods). Notably, our single-molecule measurements also reveal rapid azimuthal reorientation (i.e., "twirling") of dipoles about the DNA axis.

Figure 3A shows a representative YOYO-1 molecule bound to DNA (ω = 45°) in regime 3. The excitation laser was toggled between *x*/*y* polarization after each successive camera frame. For DNA oriented at ω = 45°, the fluorescence emission is either highly *x* or *y* polarized, depending on the excitation polarization. In contrast, for ω = 0°, the magnitudes $|{}_{x,y}P|$ are severely reduced (Fig. 3B). By fitting this dataset of single-molecule polarizations to our theoretical model (introduced

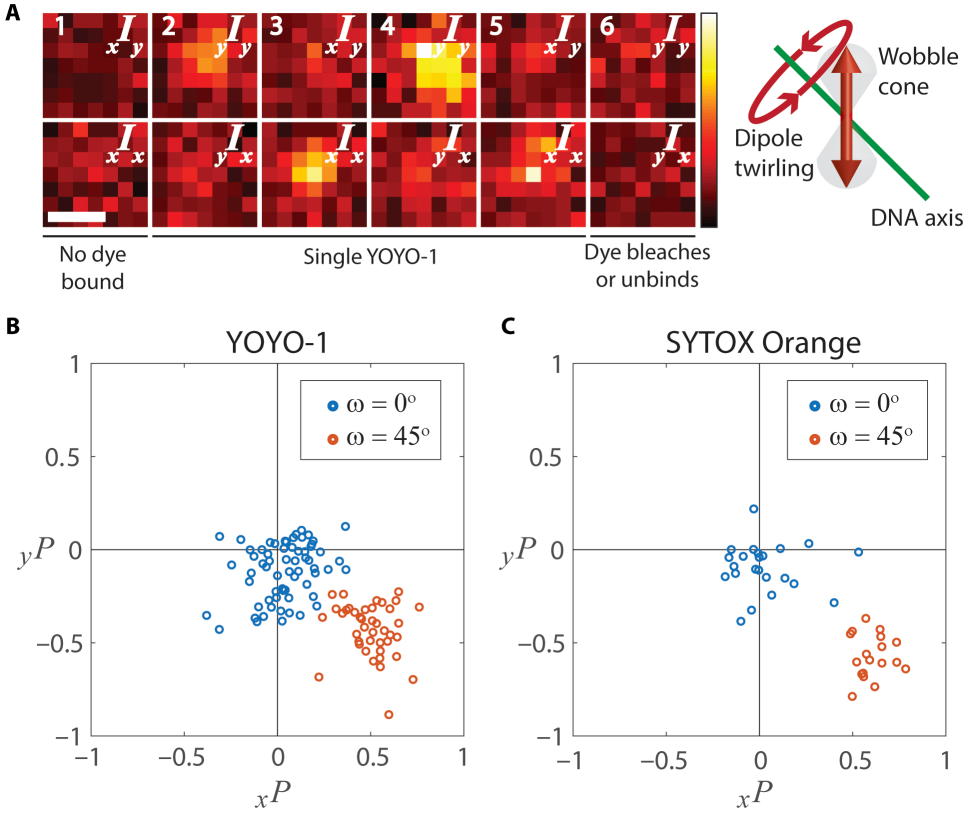

Fig. 3. DNA intercalators tilt and twirl beyond the OST. (**A**) Polarized image pairs of a single YOYO-1 molecule bound to DNA oriented at ω = 45° in regime 3 alternately excited with *x*- and *y*-polarized light (scale bar, 500 nm). A single molecule is detected in image pairs 2 to 5. Illustration: When a dipole twirls, its mean azimuthal orientation with respect to the DNA axis changes. Thus, the dipole is only efficiently excited when it rotates through the axis of the excitation polarization. Hence, toggling between *x*/*y*-polarized excitation strongly biases the emission polarization, as seen in, e.g., polarized image pairs 3 and 4. (**B** and **C**) Polarization scatterplots of single YOYO-1 (B) and SYTOX Orange (C) dyes bound to DNA oriented at ω = 0° and ω = 45° in regime 3.

above), we estimate θ = 53.9° ± 0.5°, α = 29.8° ± 1.1°. We note that under these conditions, the estimated α is smaller than the value obtained under higher dye concentration and low salt (29.1° as opposed to 39.1°). The reduced concentration of bound dye molecules may serve to minimize energy transfer between adjacent dyes. To confirm that the above results are not biased by the fact that YOYO-1 is a bis-intercalator (and the two chromophores may be alternately excited), we repeated these experiments using the mono-intercalator SYTOX Orange. This comparison yielded similar results {θ = 53.3° ± 0.7°, α = 21.4° ± 1.9°}. The narrower cone angle (α) estimated for SYTOX Orange may be due to energy transfer between the YOYO-1 chromophores (*30*) and the absence thereof for a mono-intercalator.

These single-molecule measurements provide new insight into the Brownian fluctuations of stretched DNA: For a single dipole to alternately exhibit *x*- or *y*-polarized emission upon toggling the excitation polarization (Fig. 3A), it must rotate azimuthally (along the ϕ coordinate; see fig. S2) about the DNA axis on a time scale much faster than the camera frame rate (1 s), yet slower than the fluorescence lifetime (~3 ns) (*30*). It should be noted that the rotational diffusion of the trapped beads is negligible on the time scale of the observed dye reorientation (*14*). Therefore, we conclude that such twirling reflects the intrinsic thermal fluctuations of the DNA (*31*), which has a rotational correlation time estimated to be on the order of ~100 ns (see section S7).

Intercalator tilting coincides with the end of the OST

We next seek to unravel whether the observed θ ~ 54° tilted intercalator configuration identified in regime 3 arises due to a distinct configurational state of stretched DNA or if the dye can adopt a continuum of possible tilt angles in a stretch-dependent fashion. To this end, using the high-salt buffer favoring S-DNA formation and dye concentrations in which single intercalators were resolved, we map the fluorescence polarization in regimes 2 and 3 (averaged over all single-molecule events) as a function of force beyond the OST for horizontally aligned DNA (ω = 0°; Fig. 4A), using unpolarized illumination (see Materials and Methods and section S8 for details). These results show a transition from polarized emission throughout regime 2 to depolarized emission at the onset of regime 3 at forces ~7 pN above the OST. At forces greater than 7 pN above the OST, emission polarization values saturate near $P = -0.04$ (Fig. 4A), which corresponds to the expected emission polarization for the model parameters: {θ = 53.9°, α = 29.8°} (our theoretical model was modified to account for the fact that unpolarized illumination was used in the context of this measurement,

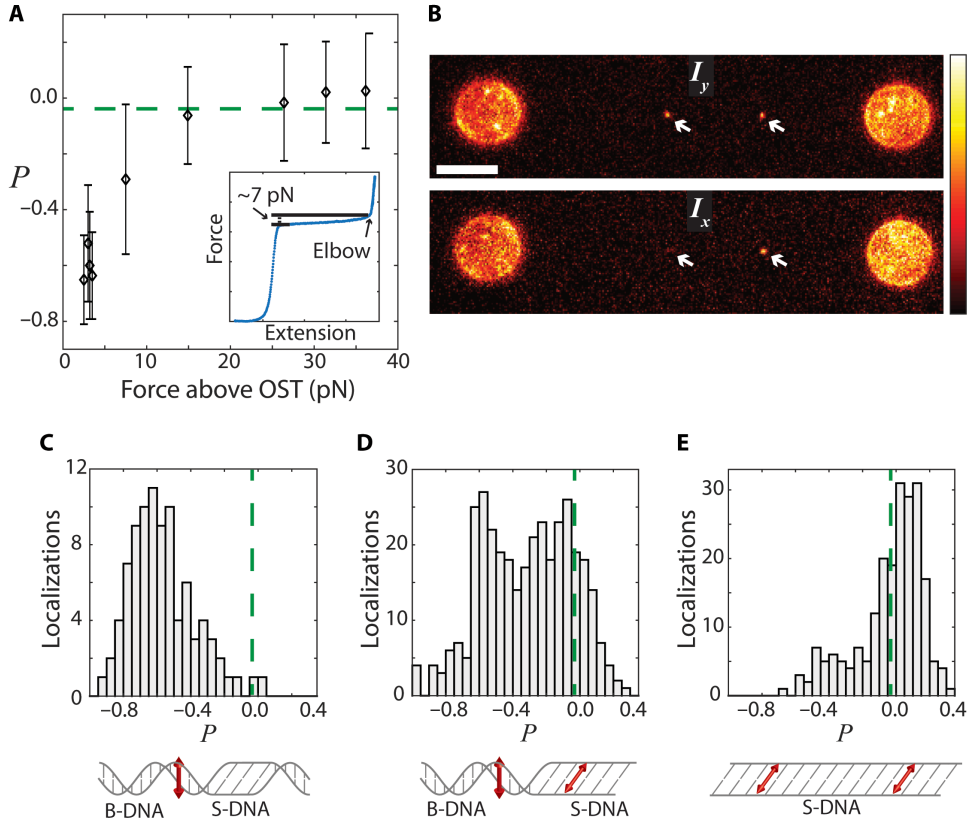

Fig. 4. Intercalator tilting occurs suddenly at the transition between regimes 2 and 3. (**A**) Average emission polarization as a function of force above the OST; data taken at extensions within the transition from regime 2 to regime 3 (vertical bars are SD). Dashed green line indicates $P = -0.04$, the emission polarization associated with model parameters {θ = 53.9°, α = 29.8°} and unpolarized excitation. Prefixes are omitted, since unpolarized excitation was used. Inset illustrates the "elbow" in the force-extension curve. (**B**) Polarization images demonstrating simultaneous detection of tilted and perpendicular YOYO-1 molecules (force ~7 pN above OST). The dye appearing brightly in both I_x and I_y channels is tilted (scale bar, 5 μm). (**C** to **E**) Single-intercalator polarization histograms at forces of 3 pN (C), 7 pN (D), and 35 pN (E) above the onset of the OST. Illustrations depict the proposed mechanism for intercalator tilting: In regime 2 (C), extended tracts of both B-DNA and S-DNA exist, and intercalated sections are primarily flanked by B-DNA and align perpendicular to the DNA axis. At the interface between regimes 2 and 3 (D), where less B-DNA is present, both perpendicular and tilted intercalators are present, flanked by B-DNA and S-DNA, respectively. Beyond the OST (E), when little or no B-DNA remains, all intercalated dipoles are forced to assume a tilted orientation, since they can now only be flanked by S-DNA.

as opposed to purely linear *x*/*y*-polarized excitation). Furthermore, at the boundary of regimes 2 and 3 (corresponding to the end of the OST, signified by the "elbow" in the force-extension curve; see inset in Fig. 4A), both populations appear to coexist (Fig. 4B). This is substantiated by histograms (Fig. 4, C to E) mapping single dye polarization values at tensions before, during, and after the end of the OST.

DISCUSSION

The novel polarization imaging methods introduced here allow us to discover structural features associated with DNA overstretching. At tensions below the OST (regime 1), where the DNA is purely B-form in nature, π-stacking interactions align intercalated dipoles perpendicular to the DNA axis. Within the OST (regime 2), because of the energy penalties incurred at interfaces between intercalated DNA and overstretched DNA, it is energetically unfavorable for intercalators to be flanked by S-DNA compared with B-DNA (*16*). As a result, intercalators are known to exhibit a much lower binding affinity for S-DNA than B-DNA. Intercalators will thus primarily be associated with B-DNA domains (i.e., perpendicular to the DNA axis) even during the OST, as long as there is still some B-DNA remaining. Only near the end of the OST (regime 3) (i.e., when there is little or no B-DNA remaining) do we observe a nongradual transition to a well-defined tilting angle of the dye from $\theta \sim 90°$ to $\theta \sim 54°$ (see Fig. 4D and section S9). This transition is exclusively observed under conditions in which intercalated DNA can only be flanked by S-DNA (i.e., relatively high coverage/low salt in Fig. 1 and low coverage/high salt in Figs. 3 and 4). Furthermore, these observations are independent of the type of intercalator used (i.e., both mono- and bis-intercalators). Altogether, while intercalators bias the relative ratio of B-DNA versus S-DNA, there is good evidence to suggest that intercalation itself does not substantially influence base pair tilt (see section S2).

We caution that a limitation of our approach is the fact that we do not directly measure the orientations of the DNA base pairs—rather, we determine the alignments of neighboring intercalated dye molecules. We cannot fully exclude the possibility that the exact base pair inclination of S-DNA could be somewhat perturbed by the presence of intercalators. Nevertheless, our data do suggest that S-DNA exhibits a tilted conformation. It has long been speculated that extension of DNA is accompanied by inclination of the individual base pairs (*5*, *6*, *35*). Moreover, at extensions near the end of the OST, computational molecular modeling studies (*5*, *36*, *37*) have predicted substantial base pair inclinations. Thus, our unique approach has, to our knowledge, provided the first experimental evidence of inclined base pairs in mechanically stretched DNA and allowed us to build a clearer understanding of S-DNA, in addition to its biological implications (*11*). More generally, the combination of fluorescence polarization imaging and DNA manipulation can provide a structural basis for the DNA conformation changes that enable genomic transactions and biotechnological processing of DNA.

MATERIALS AND METHODS

DNA and imaging buffers

For all experiments, a λ-phage DNA construct described previously (*7*) was used, which featured multiple biotins on each end to facilitate stretching to high tensions. The DNA was attached by its 3′ ends to 4.65-μm-diameter streptavidin-coated microspheres (Spherotech). Hence, this construct was topologically open and torsionally unconstrained. For experiments conducted at high-salt concentration and low dye coverage, we used a buffer containing 1 M NaCl, 20 mM Hepes (pH 7.5), 0.02% Tween 20, combined with <1 nM YOYO-1 or SYTOX Orange. The high-salt buffer served to ensure that S-DNA formation was favored over DNA melting upon overstretching. For ensemble experiments at low-salt concentration and relatively high dye coverage, we used 10 mM NaCl, 10 mM Hepes (pH 7.5), and ~10 nM YOYO-1. The differences in salt concentration further served to regulate intercalator kinetics and determine whether single dye molecules were spatially resolvable. Both YOYO-1 and SYTOX Orange were purchased from Thermo Fisher Scientific.

Optical trapping and force-extension measurements

The combined optical trapping/fluorescence microscope setup used for imaging and force spectroscopy have been described in previous publications (*7*). A multichannel flow cell (Micronit Microfluidics BV) was used to prepare DNA-bead dumbbells and facilitate rapid exchange between different buffer solutions. Once these dumbbells were assembled, the foci of the trapping beams were repositioned within the image plane using instrumentation control software written in LabVIEW (National Instruments). Using this software, DNA was stretched at an arbitrary orientation within the image plane. Force measurements were performed using back focal plane interferometry (*38*) and were displayed by the instrument control software in real time. This permitted adjustment of the extension and tension of individual DNA molecules. Minor changes in instrument calibration over time caused the tension measurement associated with the beginning of the OST (nominally 65 pN) to vary by a few piconewtons from DNA molecule to DNA molecule. Hence, the force measurements in Fig. 4B are reported relative to the force measured for the same DNA molecule at 20-μm extension ($L/L_c \sim 1.21$, near the start of the OST).

Polarization microscopy

Polarized illumination (*25*–*27*) was achieved using an EOM (model 350-80, Conoptics). Using a polarizer (Thorlabs, model: LPVISA050-MP2), an incident laser beam was linearly polarized at the EOM input. The EOM effectively acted as a voltage-controlled waveplate oriented at 45° relative to the input polarization. By applying the correct voltages on the EOM, output light was rotated either 0° or 90°, corresponding to *x*/*y*-polarized light within the microscope image plane. The EOM was synchronized to the fluorescence imaging camera using an NI-DAQ (National Instruments), and the polarization state was toggled during the pixel readout period following each successive camera exposure. Polarized laser light was focused into the back aperture of the objective, producing collimated, widefield illumination through the image plane. A liquid crystal retarder (Thorlabs, model: LCC2415-VIS) was inserted at the output of the EOM and adjusted manually to compensate for dichroics and dielectric mirrors placed in the illumination pathway. The polarization state at the image plane was measured using a polarimeter (Thorlabs, model: PAX1000VIS) balanced on the microscope stage directly above the objective and flow cell. Typically, polarization ratios ranging from ~130:1 to ~350:1 were achieved, and the polarization was aligned to the *x*/*y* axes within ~3°. For measurements in which unpolarized illumination was desired (see Fig. 4), the EOM was toggled between *x*- and *y*-polarized illumination at a rate of 1 ms. Since the camera frame rate was 1 s for all experiments involving YOYO-1, this ensured that all dipoles lying within the image plane were efficiently excited over the course of a single camera exposure. Since the excitation efficiency is proportional to the cosine-square of the angle

between the absorption dipole moment and the excitation polarization, toggling between purely *x*/*y*-polarized excitation will achieve an effect identical to exciting with a continuously rotated excitation polarization or using circularly polarized illumination (see section S8).

For polarized detection of fluorescence emission, an OptoSplit III (Cairn Research) with a polarizing beamsplitter module (part number: P290/POL/001) was used to simultaneously project *x*/*y*-polarized light onto separate regions of the camera sensor. Per recommendation from the manufacturer, a cleanup linear polarizer (P290/POL/002) was also placed in the reflected S polarization channel (*x* polarization channel with respect to the image plane coordinates). However, these optics reduced the ratio R_{em} of overall light efficiency of the S polarization channel relative to the P channel and called for an additional calibration step to accurately measure emission polarizations: First, it was necessary to determine the ratio R_{ex} of the power of *x*-polarized versus *y*-polarized excitation light transmitted to the image plane. Dye solution was run through the flow cell and imaged over successive frames while alternating between *x*/*y*-polarized excitation. This set of images was recorded without using the polarizing beamsplitter. The ratio of dark-count–subtracted summed intensities over the field of view (i.e., the sum of the camera pixel ADC counts) using either excitation polarization was used to determine R_{ex}. Next, a new set of images was acquired using the polarizing beamsplitter and cleanup polarizer. For a given emission channel, the dark-count–subtracted summed intensity using both *x*- and *y*-polarized illumination was determined. Using the same prefix/suffix notation to indicate excitation/emission polarizations, we denote this set of intensity measurements as ${}_{x,y}I^{unc}_{x,y}$, where the superscript "unc" denotes that the intensity measurements have not been corrected for transmission/reflection efficiency. The ratio R_{em} was computed as

$$R_{em} = \frac{R_{ex}\,{}_xI^{unc}_y + {}_yI^{unc}_y}{R_{ex}\,{}_xI^{unc}_x + {}_yI^{unc}_x} \quad (2)$$

Typical measured values for R_{em} were around ~1.3 to 1.5. To accurately compute the polarizations ${}_{x,y}P$, we used the formulas

$$\begin{aligned} {}_xI_x &= R_{em}\,{}_xI^{unc}_x;\;\; {}_xI_y = {}_xI^{unc}_y \\ {}_yI_x^{\;y} &= R_{em}\,{}_yI^{unc}_x;\;\; {}_yI_y = {}_yI^{unc}_y \end{aligned} \quad (3)$$

The corrected intensities were then used as inputs to Eq. 1. Displayed representative images of *x*-polarized fluorescence images were also multiplied by the factor R_{em}.

Fluorescence imaging

All imaging was conducted using the same 1.2 numerical aperture/60× Nikon objective used for optical trapping. Fluorescence was recorded on an electron-multiplying charge-coupled device camera (iXON+ 897E, Andor Technology). The camera was controlled using the Solis software package provided by the manufacturer. For bulk imaging experiments conducted at low ionic strength, trapped DNA constructs were immediately moved into the flow cell channel containing dye solution, and the DNA was then stretched to the desired extension and imaged using a laser intensity of ~1 W/cm^2. Camera exposure times were set to 1 s, using an electron-multiplying gain of 300, while the excitation polarization was toggled after each frame. To produce an emission polarization estimate, intensity values were averaged over three frames using the same excitation polarization. Hence, a total of six consecutive exposures were required to produce estimates of both ${}_xP$ and ${}_yP$ for a given DNA orientation ω. For single-molecule imaging experiments conducted at high ionic strength, bare DNA was first stretched to the desired extension and then moved to the mouth of the flow cell channel containing dye solution. By manually moving the DNA deeper into the dye channel, the local concentration of intercalators could be adjusted, until frequent single-intercalator binding events were discernable. For single-molecule imaging, we used a laser intensity of ~250 W/ cm^2. For experiments involving YOYO-1, camera exposures were set to 1-s duration. For SYTOX Orange, an 85-ms framerate was used because of its rapid unbinding rate. As in the bulk experiments, we used an EM gain of 300, and the excitation polarization was toggled after each successive exposure. To acquire both a ${}_xP$ and ${}_yP$ measurement for a single molecule, it was necessary to detect the same dye molecule over at least two consecutive frames. For excitation of YOYO-1 and SYTOX Orange, a 491-nm, 50-mW CW Cobolt Calypso and a 532-nm, 50-mW CW Cobolt Samba laser were used, respectively. To image YOYO-1, an FF01-R488 dichroic beamsplitter and an FF-525/50 bandpass filter (Semrock Inc.) were used. To image SYTOX Orange, a z532rdc dichroic beamsplitter (Chroma Technology) and an FFO1-580/60 bandpass filter (Semrock Inc.) were used.

Image processing

To calculate emission polarizations of densely labeled DNA from bulk fluorescence images, a region of interest (ROI) was manually drawn around images of intercalated DNA. For details of how ROIs were constructed for ensemble measurements, see section S10. Background-subtracted signal measured in the *x*-polarized emission channel was multiplied by the correction factor R_{em} (described above), and emission polarizations ${}_{x,y}P$ were calculated using Eq. 1. The DNA orientations ω were measured directly from raw image data using the software ImageJ (available for download at https://imagej.nih.gov/ij/). Data processing was performed using custom scripts written in MATLAB (MathWorks). A drawback of our chosen experimental approach is the fact that variation in the excitation laser spot throughout the field of view can introduce changes in emitted intensity, as the DNA is rotated to different spatial locations. Furthermore, manually rotating the DNA is a time-consuming process, and dye bleaching/unbinding can alter total detected fluorescence intensity. For these reasons, we instead chose to focus our analysis on emission polarization ratios. Polarization ratios are self-referencing measurements. Hence, factors influencing total emitted fluorescence are not expected to distort our results.

To calculate emission polarizations of single intercalators, raw image data were processed using custom MATLAB scripts for detecting and localizing single fluorescent molecules. The total intensity for a given molecule localized in a particular polarization channel was determined by summing the pixel intensities contained in a 5 × 5 pixel box centered on the coordinates of the localized molecule and subtracting background fluorescence estimated from nearby pixel intensities not containing any localized molecules. Using the affine transformation described above, the coordinates of the molecule in the alternate polarization channel were estimated, and the intensity of the molecule in the alternate channel was computed using the same procedure. Intensity estimates computed from the *x* polarization channel were multiplied by the correction factor R_{em}, and ${}_{x,y}P$ estimates were computed using Eq. 1. To produce the scatterplots in Fig. 3 (B and C), single intercalators were identified in ≥2 consecutive

camera frames (excited using both *x*- and *y*-polarized illumination). Localizations were assumed to originate from the same molecule if they were localized less than 1 pixel (130 nm) apart over consecutive frames, and intensity estimates for a given molecule using the same illumination polarization were summed over multiple frames to produce the most precise estimates of ${}_{x,y}P$.

Systematic single-molecule localization errors may result when fluorescence is detected from emitting dipoles tilted out of the microscope image plane (*39*–*41*). Exceptionally large (>130 nm, or one camera pixel) localization errors could cause fluorescence emission from different molecules appearing in the *x*/*y*-polarized emission channels to be improperly matched, or introduce uncertainty as to whether the same molecule is appearing over multiple sequential camera frames. To minimize dipole orientation–induced single-molecule localization errors (*39*–*41*), we used two strategies: (i) By constraining the excitation polarization within the image plane, we ensure that excited dipoles will predominantly also lie in this plane—localization errors are minimal for dipoles that are not inclined toward the *z* axis. (ii) The optical tweezers ensure that the intercalated DNA is located close to the microscope's nominal focal plane—localization errors become prominent only when imaging moderately defocused molecules.

Statistical analysis

Once values of ${}_{x,y}P$ versus ω were obtained, these data were fit to a theoretical model (see section S2) to estimate the underlying tilt/wobble parameters {θ, α}. Fitting was performed using the nonlinear least squares estimation function `nlinfit()` provided in MATLAB. To determine standard errors of estimated parameters, an estimated covariance matrix for {θ, α} was also computed using `nlinfit()` (*42*). Briefly, the standard error bounds for the estimated parameters were determined from the mean square error between the measured data and the fitted model function, the model function Jacobian, and the number of collected data points. For measurements recorded using high labeling density and low salt, estimates of the parameters {θ, α} were based on $N = 44$ emission polarization measurements taken using a unique DNA orientation ω or excitation polarization for DNA extended within the OST (regime 2), and $N = 66$ emission polarization measurements for DNA extended beyond the OST (regime 3). To estimate the precision with which a single polarization ratio could be obtained, we calculated the root mean square deviation between the fitted model and the polarization data. This yielded an estimated precision of $\sigma_P = 0.16$. In addition to degraded precision, noise from high background imaging conditions can introduce some bias in measured polarization ratios, even after appropriate background subtraction has been performed. To investigate the amount of bias we could potentially incur, we simulated ratios of Poisson-distributed random variables to mimic low signal/high background imaging conditions. We found that in conditions in which the precision of individual polarization measurements was $\sigma_P = 0.16$, expected bias was approximately ~0.01 (about an order of magnitude smaller than the inherent precision). Hence, we do not expect polarization estimation biases to strongly affect the inferred parameters {θ, α}. For densely labeled DNA extended within the OST (regime 2), ${}_xP$ data were excluded from analysis for ω = 0° to 20°, as were ${}_yP$ measurements for ω = 70° to 90°. At these DNA orientations, the excitation polarization was nearly parallel to the DNA axis, and insufficient fluorescence signal was recorded to produce reliable polarization measurements.

Using low labeling density and a high-salt imaging buffer, our estimates of the parameters {θ, α} are based on $N = 107$ YOYO-1 molecules and $N = 41$ SYTOX Orange molecules. The same theoretical model and fitting procedure based on nonlinear least squares that were used to analyze high labeling density measurements were used. For each dye (YOYO-1 or SYTOX Orange, respectively), the polarization measurement precision (per molecule) was estimated as the root-mean-square deviation between the experimental polarization values and the fitted model function. For YOYO-1, we estimated $\sigma_P = 0.15$, and for SYTOX Orange, we estimated $\sigma_P = 0.16$. The single-molecule emission polarization data (recorded using unpolarized excitation illumination) presented in Fig. 4A are based on a total of $N = 1368$ localizations.

SUPPLEMENTARY MATERIALS

Supplementary material for this article is available at http://advances.sciencemag.org/cgi/content/full/5/3/eaav1083/DC1

Fig. S1. Intercalator tilting is inhibited when dye coverage is high.
Fig. S2. Summary of different modes of rotational motion.
Fig. S3. Definitions of coordinate systems and reference frames.
Fig. S4. The effect of wobble and tilt upon emission polarization.
Fig. S5. Three experimental configurations for measuring intercalated dye orientations.
Fig. S6. Simulated measurements corresponding to parameter sets {θ = 85°, α = 85°} and {θ = 53.6°, α = 39.1°}.
Fig. S7. Intuitive description of the differences between experimental configurations.
Fig. S8. Example ROI used for ensemble fluorescence polarization measurements.
Table S1. Accounting for energy transfer.
Section S1. Intercalators prevent peeling and bubble formation under low-salt conditions
Section S2. Relating the measured intercalator orientation to DNA structure
Section S3. Theoretical model: Tilt wobble and twirl
Section S4. Distinguishing wobble and tilt
Section S5. Why is it necessary to rotate the DNA?
Section S6. The effect of energy transfer upon emission polarization
Section S7. How rapidly do intercalators twirl?
Section S8. Rapidly toggling between *x*-/*y*-polarized illumination is equivalent to unpolarized excitation within the image plane
Section S9. Because of reduced intercalator affinity for S-DNA, tilting is only observed at the end of the OST
Section S10. ROI selection for ensemble fluorescence polarization measurements
References (*43*–*60*)

REFERENCES AND NOTES

1. C. Bustamante, Z. Bryant, S. B. Smith, Ten years of tension: Single-molecule DNA mechanics. *Nature* **421**, 423–427 (2003).
2. T. Paramanathan, I. Vladescu, M. J. McCauley, I. Rouzina, M. C. Williams, Force spectroscopy reveals the DNA structural dynamics that govern the slow binding of Actinomycin D. *Nucleic Acids Res.* **40**, 4925–4932 (2012).
3. M. R. Jones, N. C. Seeman, C. A. Mirkin, Programmable materials and the nature of the DNA bond. *Science* **347**, 1260901 (2015).
4. J. D. Watson, F. H. C. Crick, Molecular structure of nucleic acids. *Nature* **171**, 737–738 (1953).
5. P. Cluzel, A. Lebrun, C. Heller, R. Lavery, J.-L. Viovy, D. Chatenay, F. Caron, DNA: An extensible molecule. *Science* **271**, 792–794 (1996).
6. S. B. Smith, Y. Cui, C. Bustamante, Overstretching B-DNA: The elastic response of individual double-stranded and single-stranded DNA molecules. *Science* **271**, 795–799 (1996).
7. J. van Mameren, P. Gross, G. Farge, P. Hooijman, M. Modesti, M. Falkenberg, G. J. L. Wuite, E. J. G. Peterman, Unraveling the structure of DNA during overstretching by using multicolor, single-molecule fluorescence imaging. *Proc. Natl. Acad. Sci. U.S.A.* **106**, 18231–18236 (2009).
8. N. Bosaeus, A. El-Sagheer, T. Brown, S. B. Smith, B. Åkerman, C. Bustamante, B. Nordén, Tension induces a base-paired overstretched DNA conformation. *Proc. Natl. Acad. Sci. U.S.A.* **109**, 15179–15184 (2012).
9. G. A. King, P. Gross, U. Bockelmann, M. Modesti, G. J. L. Wuite, E. J. G. Peterman, Revealing the competition between peeled ssDNA, melting bubbles, and S-DNA during DNA overstretching using fluorescence microscopy. *Proc. Natl. Acad. Sci. U.S.A.* **110**, 3859–3864 (2013).
10. J. F. Léger, G. Romano, A. Sarkar, J. Robert, L. Bourdieu, D. Chatenay, J. F. Marko, Structural transitions of a twisted and stretched DNA molecule. *Phys. Rev. Lett.* **83**, 1066–1069 (1999).

11. N. Bosaeus, A. Reymer, T. Beke-Somfai, T. Brown, M. Takahashi, P. Wittung-Stafshede, S. Rocha, B. Nordén, A stretched conformation of DNA with a biological role? *Q. Rev. Biophys.* **50**, e11 (2017).
12. X. Zhang, H. Chen, S. Le, I. Rouzina, P. S. Doyle, J. Yan, Revealing the competition between peeled ssDNA, melting bubbles, and S-DNA during DNA overstretching by single-molecule calorimetry. *Proc. Natl. Acad. Sci. U.S.A.* **110**, 3865–3870 (2013).
13. I. D. Vladescu, M. J. McCauley, M. E. Nuñez, I. Rouzina, M. C. Williams, Quantifying force-dependent and zero-force DNA intercalation by single-molecule stretching. *Nat. Methods* **4**, 517–522 (2007).
14. P. Gross, N. Laurens, L. B. Oddershede, U. Bockelmann, E. J. G. Peterman, G. J. L. Wuite, Quantifying how DNA stretches, melts, and changes twist under tension. *Nat. Phys.* **7**, 731–736 (2011).
15. A. S. Biebricher, I. Heller, R. F. H. Roijmans, T. P. Hoekstra, E. J. G. Peterman, G. J. L. Wuite, The impact of DNA intercalators on DNA and DNA-processing enzymes elucidated through force-dependent binding kinetics. *Nat. Commun.* **6**, 7304 (2015).
16. K. Schakenraad, A. S. Biebricher, M. Sebregts, B. Ten Bensel, E. J. G. Peterman, G. J. L. Wuite, I. Heller, C. Storm, P. van der Schoot, Hyperstretching DNA. *Nat. Commun.* **8**, 2197 (2017).
17. D. Y. Shroder, L. G. Lippert, Y. E. Goldman, Single molecule optical measurements of orientation and rotations of biological macromolecules. *Methods Appl. Fluoresc.* **4**, 042004 (2016).
18. M. Böhmer, J. Enderlein, Orientation imaging of single molecules by wide-field epifluorescence microscopy. *J. Opt. Soc. Am. B* **20**, 554–559 (2003).
19. M. P. Backlund, M. D. Lew, A. S. Backer, S. J. Sahl, W. E. Moerner, The role of molecular dipole orientation in single-molecule fluorescence microscopy and implications for super-resolution imaging. *ChemPhysChem* **15**, 587–599 (2014).
20. O. Zhang, J. Lu, T. Ding, M. D. Lew, Imaging the three-dimensional orientation and rotational mobility of fluorescent emitters using the Tri-spot point spread function. *Appl. Phys. Lett.* **113**, 031103 (2018).
21. C. U. Murade, V. Subramaniam, C. Otto, M. L. Bennink, Force spectroscopy and fluorescence microscopy of dsDNA–YOYO-1 complexes: Implications for the structure of dsDNA in the overstretching region. *Nucleic Acids Res.* **38**, 3423–3431 (2010).
22. C. A. Valades-Cruz, H. A. Shaban, A. Kress, N. Bertaux, S. Monneret, M. Mavrakis, J. Savatier, S. Brasselet, Quantitative nanoscale imaging of orientational order in biological filaments by polarized superresolution microscopy. *Proc. Natl. Acad. Sci. U.S.A.* **113**, E820–E828 (2016).
23. A. S. Backer, M. Y. Lee, W. E. Moerner, Enhanced DNA imaging using super-resolution microscopy and simultaneous single-molecule orientation measurements. *Optica* **3**, 659–666 (2016).
24. J. van Mameren, K. Vermeulen, G. J. L. Wuite, E. J. G. Peterman, A polarized view on DNA under tension. *J. Chem. Phys.* **148**, 123306 (2018).
25. T. Ha, Th. Enderle, D. S. Chemla, P. R. Selvin, S. Weiss, Single molecule dynamics studied by polarization modulation. *Phys. Rev. Lett.* **77**, 3979–3982 (1996).
26. H. Sosa, E. J. G. Peterman, W. E. Moerner, L. S. B. Goldstein, ADP-induced rocking of the kinesin motor domain revealed by single-molecule fluorescence polarization microscopy. *Nat. Struct. Biol.* **8**, 540–544 (2001).
27. E. J. G. Peterman, H. Sosa, L. S. B. Goldstein, W. E. Moerner, Polarized fluorescence microscopy of individual and many kinesin motors bound to axonemal microtubules. *Biophys. J.* **81**, 2851–2863 (2001).
28. T. J. Gould, M. S. Gunewardene, M. V. Gudheti, V. V. Verkhusha, S.-R. Yin, J. A. Gosse, S. T. Hess, Nanoscale imaging of molecular positions and anisotropies. *Nat. Methods* **5**, 1027–1030 (2008).
29. H. A. Shaban, C. A. Valades-Cruz, J. Savatier, S. Brasselet, Polarization super-resolution structural imaging inside amyloid fibrils using Thioflavine T. *Sci. Rep.* **7**, 12482 (2017).
30. C. Carlsson, A. Larsson, M. Jonsson, B. Albinsson, B. Nordén, Optical and photophysical properties of the oxazole yellow DNA probes YO and YOYO. *J. Phys. Chem.* **98**, 10313–10321 (1994).
31. M. D. Barkley, B. H. Zimm, Theory of twisting and bending of chain macromolecules; analysis of the fluorescence depolarization of DNA. *J. Chem. Phys.* **70**, 2991–3007 (1979).
32. J. Lipfert, M. M. van Oene, M. Lee, F. Pedaci, N. H. Dekker, Torque spectroscopy for the study of rotary motion in biological systems. *Chem. Rev.* **115**, 1449–1474 (2015).
33. M. Irving, Steady-state polarization from cylindrically symmetric fluorophores undergoing rapid restricted motion. *Biophys. J.* **70**, 1830–1835 (1996).
34. J. E. T. Corrie, B. D. Brandmeier, R. E. Ferguson, D. R. Trentham, J. Kendrick-Jones, S. C. Hopkins, U. A. van der Heide, Y. E. Goldman, C. Sabido-David, R. E. Dale, S. Criddle, M. Irving, Dynamic measurement of myosin light-chain-domain tilt and twist in muscle contraction. *Nature* **400**, 425–430 (1999).
35. M. H. F. Wilkins, R. G. Gosling, W. E. Seeds, Physical studies of nucleic acid: Nucleic acid: an extensible molecule? *Nature* **167**, 759–760 (1951).
36. M. W. Konrad, J. I. Bolonick, Molecular dynamics simulation of DNA stretching is consistent with the tension observed for extension and strand separation and predicts a novel ladder structure. *J. Am. Chem. Soc.* **118**, 10989–10994 (1996).
37. K. M. Kosikov, A. A. Gorin, V. B. Zhurkin, W. K. Olson, DNA stretching and compression: Large-scale simulations of double helical structures. *J. Mol. Biol.* **289**, 1301–1326 (1999).
38. F. Gittes, C. F. Schmidt, Interference model for back-focal-plane displacement detection in optical tweezers. *Opt. Lett.* **23**, 7–9 (1998).
39. S. Stallinga, B. Rieger, Accuracy of the gaussian point spread function model in 2D localization microscopy. *Opt. Express* **18**, 24461–24476 (2010).
40. M. P. Backlund, A. Arbabi, P. N. Petrov, E. Arbabi, S. Saurabh, A. Faraon, W. E. Moerner, Removing orientation-induced localization biases in single-molecule microscopy using a broadband metasurface mask. *Nat. Photonics* **10**, 459–462 (2016).
41. M. D. Lew, M. P. Backlund, W. E. Moerner, Rotational mobility of single molecules affects localization accuracy in super-resolution fluorescence microscopy. *Nano Lett.* **13**, 3967–3972 (2013).
42. G. A. F. Seber, C. J. Wild, *Nonlinear Regression* (Wiley-Interscience, 2003).
43. H. Ihmels, D. Otto, Intercalation of Organinc Dye Molecules into Double Stranded DNA-General Principles and Recent Developments, in *Supramolecular Dye Chemistry*, F. Würthner, Ed. (Springer, 2005), pp. 161–204.
44. F. Johansen, J. P. Jacobsen, ^{1}H NMR studies of the bis-intercalation of a homodimeric oxazole yellow dye in DNA oligonucleotides. *J. Biomol. Struct. Dyn.* **16**, 205–222 (1998).
45. K. Kinosita Jr., S. Kawato, A. Ikegami, A theory of fluorescence polarization decay in membranes. *Biophys. J.* **20**, 289–305 (1977).
46. G. Lipari, A. Szabo, Effect of librational motion on fluorescence depolarization and nuclear magnetic resonance relaxation in macromolecules and membranes. *Biophys. J.* **30**, 489–506 (1980).
47. R. E. Dale, S. C. Hopkins, U. A. an der Heide, T. Marszałek, M. Irving, Y. E. Goldman, Model-independent analysis of the orientation of fluorescent probes with restricted mobility in muscle fibers. *Biophys. J.* **76**, 1606–1618 (1999).
48. J. N. Forkey, M. E. Quinlan, M. A. Shaw, J. E. T. Corrie, Y. E. Goldman, Three-dimensional structural dynamics of myosin V by single-molecule fluorescence polarization. *Nature* **422**, 399–404 (2003).
49. J. N. Forkey, M. E. Quinlan, Y. E. Goldman, Measurement of single macromolecule orientation by total internal reflection fluorescence polarization microscopy. *Biophys. J.* **89**, 1261–1271 (2005).
50. A. S. Backer, W. E. Moerner, Determining the rotational mobility of a single molecule from a single image: A numerical study. *Opt. Express* **23**, 4255–4276 (2015).
51. A. Larsson, C. Carlsson, M. Jonsson, B. Albinsson, Characterization of the binding of the fluorescent dyes YO and YOYO to DNA by polarized light spectroscopy. *J. Am. Chem. Soc.* **116**, 8459–8465 (1994).
52. D. Axelrod, Carbocyanine dye orientation in red cell membrane studied by microscopic fluorescence polarization. *Biophys. J.* **26**, 557–573 (1979).
53. R. M. Dickson, D. J. Norris, W. E. Moerner, Simultaneous imaging of individual molecules aligned both parallel and perpendicular to the optic axis. *Phys. Rev. Lett.* **81**, 5322–5325 (1998).
54. K. I. Mortensen, L. S. Churchman, J. A. Spudich, H. Flyvbjerg, Optimized localization analysis for single-molecule tracking and super-resolution microscopy. *Nat. Methods* **7**, 377–381 (2010).
55. A. S. Backer, W. E. Moerner, Extending single-molecule microscopy using optical Fourier processing. *J. Phys. Chem. B* **118**, 8313–8329 (2014).
56. K. D. Weston, L. S. Goldner, Orientation imaging and reorientation dynamics of single dye molecules. *J. Phys. Chem. B* **105**, 3453–3462 (2001).
57. Ph. Wahl, J. Paoletti, J.-B. Le Pecq, Decay of fluorescence emission anisotropy of the ethidium bromide-DNA complex evidence for an internal motion in DNA. *Proc. Natl. Acad. Sci. U.S.A.* **65**, 417–421 (1970).
58. S. A. Allison, J. M. Schurr, Torsional dynamics and depolarization of fluorescence of linear macromolecules I. theory and application to DNAt. *Chem. Phys.* **41**, 35–59 (1979).
59. B. S. Fujimoto, J. M. Schurr, Dependence of the torsional rigidity of DNA on base composition. *Nature* **344**, 175–178 (1990).
60. P. R. Selvin, D. N. Cook, N. G. Pon, W. R. Bauer, M. P. Klein, J. E. Hearst, Torsional rigidity of positively and negatively supercoiled DNA. *Science* **255**, 82–85 (1992).

Acknowledgments

Funding: A.S.Ba. acknowledges research funding and support from the Harry S. Truman Fellowship. I.H. acknowledges research funding from an NWO VIDI award. A.S.Bi. and E.J.G.P. acknowledge research funding from the Human Frontier Science Program. G.A.K., G.J.L.W., and E.J.G.P. acknowledge research funding from the Netherlands Organization for Scientific Research (NWO; "Catching PICH in the Act," project number 741.015.002). The research leading to these results has received funding from LASERLAB-EUROPE (grant agreement no. 654148, European Union's Horizon 2020 Research and Innovation Programme). This work was supported by the Laboratory Directed Research and Development program at Sandia National Laboratories, a multimission laboratory managed and operated by the National Technology and Engineering Solutions of Sandia, LLC, a wholly owned subsidiary of Honeywell International Inc., for the U.S. Department of Energy's National Nuclear Security Administration

under contract no. DE-NA0003525. This paper describes objective technical results and analysis. Any subjective views or opinions that might be expressed in the paper do not necessarily represent the views of the U.S. Department of Energy or the U.S. government. **Author contributions:** A.S.Ba. proposed the project, collected and analyzed the data. A.S.Bi. and G.A.K. developed the instrumentation, experimental protocols, and DNA constructs. All authors contributed to the planning, design of experiments, discussion of results, and writing of the manuscript. **Competing interests:** G.J.L.W., I.H., and E.J.G.P. are co-inventors on a patent, "Method and system for imaging a molecular strand," issued in the United States (US 9,766,180), pending in Europe (PCT/NL2014/050351), which is related to this work. This patent is licensed to LUMICKS b.v., of which G.J.L.W. and E.J.G.P. are co-founders; G.J.L.W., I.H., and E.J.G.P. own stocks in LUMICKS b.v. The other authors declare that they have no competing interests. **Data and materials availability:** All data needed to evaluate the conclusions in the paper are present in the paper and/or the Supplementary Materials. Additional data related to this paper may be requested from the authors. Requests should be addressed to A.S.Ba. and E.J.G.P.

Submitted 14 August 2018
Accepted 4 February 2019
Published 22 March 2019
10.1126/sciadv.aav1083

Citation: A. S. Backer, A. S. Biebricher, G. A. King, G. J. L. Wuite, I. Heller, E. J. G. Peterman, Single-molecule polarization microscopy of DNA intercalators sheds light on the structure of S-DNA. *Sci. Adv.* **5**, eaav1083 (2019).

Science Advances

Single-molecule polarization microscopy of DNA intercalators sheds light on the structure of S-DNA

Adam S. Backer, Andreas S. Biebricher, Graeme A. King, Gijs J. L. Wuite, Iddo Heller and Erwin J. G. Peterman

Sci Adv **5** (3), eaav1083.
DOI: 10.1126/sciadv.aav1083